A tree-scattering model for improved propagation prediction in urban microcells

Document status and date:
Published: 01/01/2004

Document Version:
Publisher's PDF, also known as Version of Record (includes final page, issue and volume numbers)

Please check the document version of this publication:

• A submitted manuscript is the version of the article upon submission and before peer-review. There can be important differences between the submitted version and the official published version of record. People interested in the research are advised to contact the author for the final version of the publication, or visit the DOI to the publisher's website.
• The final author version and the galley proof are versions of the publication after peer review.
• The final published version features the final layout of the paper including the volume, issue and page numbers.

Link to publication

A Tree-Scattering Model for Improved Propagation Prediction in Urban Microcells

Yvo L. C. de Jong, *Member, IEEE,* and Matti H. A. J. Herben, *Senior Member, IEEE*

Abstract—This paper presents a model for the scattering of radiowaves from the canopy of a single tree. The canopy is modeled as a cylindrical volume containing randomly distributed and oriented cylinders, representing the branches, and thin disks, representing the leaves. A simple expression for the incoherent scattered field outside the canopy is obtained using Twersky's multiple scattering theory. This expression is shown to agree well with results of scattering measurements on a live tree typical of those found in urban environments. The scattering model can be readily incorporated in ray-based propagation prediction tools that assist the planning of microcellular radio networks. This involves the use of so-called tree-scattered rays, which interact at the tree centers. Path loss predictions generated with the aid of the new model are shown and compared with measured data to illustrate the considerable improvement in prediction accuracy that can be achieved in realistic urban microcellular scenarios by taking into account the scatter from trees.

Index Terms—Mobile communication, radio propagation, tree scattering, urban microcells, vegetation.

I. INTRODUCTION

WITH the advent of microcellular radio networks likely to be employed in third-generation mobile communication systems, there is an increased interest in propagation models that are able to provide location-specific predictions of channel parameters such as local mean power and delay spread. Ray-based propagation prediction, in which the propagation of radiowaves is described in terms of straight trajectories in space called rays, has emerged as the most successful technique for this purpose. Quasi-two-dimensional ray-based models (often just called two-dimensional, or 2-D, models) are quite adequate if transmit and receive heights are well below the average rooftop level [1], [2], as is normally the case in urban microcells. These models have been reported to provide excellent prediction results for a variety of urban scenarios. In many other cases, however, these models do not provide the same accuracy that can presently be achieved for macrocells.

Although currently available ray-tracing tools come in a wide variety with regard to the implementation of the ray-tracing algorithm itself, they are generally based on models of the same

propagation mechanisms: line-of-sight (LoS) propagation, reflection, and diffraction. In a number of frequently occurring scenarios, these mechanisms alone do not adequately explain the channel properties that are actually observed. In particular, the transmission of radiowaves through buildings is often significant behind buildings obstructing the LoS to the base station antenna [3]–[5] and, as will be shown herein, scattering from trees located near street intersections can play an important role with regard to propagation around street corners [6].

Investigations of tree effects on radio channel characteristics have hitherto been restricted mainly to coherent scattering, of which the attenuation of waves propagating through the foliage ("tree shadowing") is the most obvious manifestation [7], [8]. Incoherent (or diffuse) scattered fields—which are due to the macroscopic dielectric heterogeneity of the tree canopy—are often neglected, even though they are generally predominant over the coherent scattered field in directions other than the forward direction. In situations in which the LoS path is obstructed, and reflected and diffracted field contributions from other objects are weak, incoherent tree-scattered fields can become dominant.

This paper presents a model for the incoherent scattering from deciduous trees. As this model finds its application in propagation prediction for urban microcell environments, it is kept quasi-two-dimensional. This means that it will be assumed that the reception point and the source of the incident field are both at the same height as the center of the tree canopy and that the canopy is tall. The wave propagation is in three-dimensional (3-D) space, as usual. Furthermore, attention is restricted to the vertically polarized field components and, hence, the final expressions for the scattered fields are scalar. The tree itself is assumed to consist of a finite cylindrical volume containing randomly located and oriented branches and leaves, modeled as dielectric cylinders and disks, as in [8]–[10]. The effects of the trunk are neglected.

As in [8], the coherent field in the canopy is computed by using an effective propagation constant that is determined by the medium's equivalent scattering amplitude per unit volume in the forward scattering direction. The incoherent scattered field outside the canopy is obtained in terms of an integral over the canopy volume. The application of the resulting expression in ray-based propagation models is straightforward.

The organization of the paper is as follows. Section II describes the overall scattering geometry and the scattering from individual branches and leaves. A model for the scattering of radiowaves from an entire tree canopy is presented in Section III. Numerical results generated using this model are discussed in Section IV and a comparison with experimental
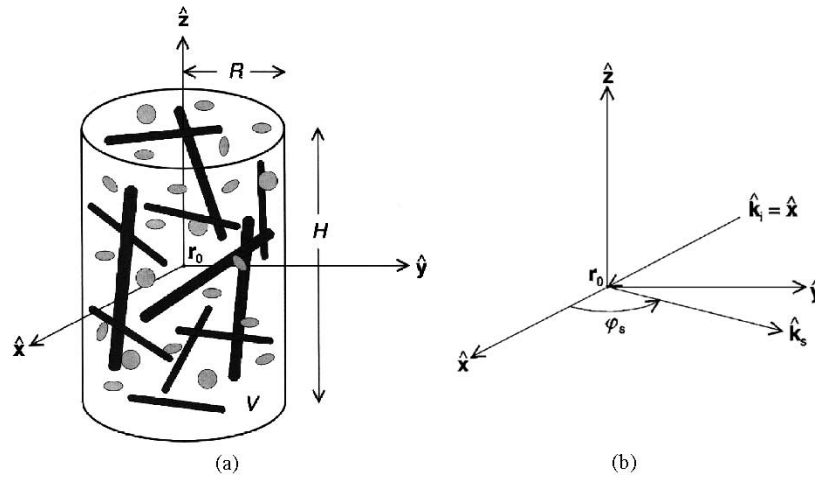
Fig. 1.   Problem geometry. (a) Canopy volume. (b) Incidence and scattering directions.

data is made in Section V. Section VI illustrates the considerable improvement in prediction accuracy that can be achieved in a realistic microcellular scenario by considering tree scattering. Conclusions are drawn in Section VII.

II. TREE MODEL

From the standpoint of radiowave propagation, a vegetation canopy is a bounded medium consisting of many discrete, randomly distributed and oriented, dielectric inclusions (branches, leaves, fruit, etc.) in a homogeneous background material (air). In general, the medium may be random in both space and time, but, in the present study, the canopy structure and the scattered field are assumed to be time invariant. At frequencies used for terrestrial mobile communications, which are in the range from 0.8 to 2.2 GHz, the dimensions of the inclusions can be comparable to or larger than the wavelength. This means that the canopy cannot be treated as a macroscopically homogeneous dielectric mixture, characterized by an effective permittivity. Instead, the geometries and orientations of the various types of inclusions present in the canopy also have to be taken into account.

In the present study, a tree canopy is assumed to consist of an ensemble of leaves and branches. Leaves are modeled as thin lossy dielectric disks and branches as finite lossy dielectric cylinders. A consequence of the dielectric heterogeneity of the canopy volume is that the scattered field has an incoherent component, which consists of uncorrelated contributions from the individual scatterers. For short propagation paths through random media, the incoherent scattered field in the forward direction is generally small as compared with the coherent scattered field. For this reason, the incoherent scattered field is often disregarded in the literature dealing with tree scattering (attenuation) effects in terrestrial radiowave propagation. However, in scattering directions other than the forward direction, the incoherent field is much more important than the coherent field.

A. Overall Problem Geometry

An illustration of the tree model adopted in this study is given in Fig. 1. The tree's canopy is modeled as a vertically oriented cylindrical volume V in a rectangular coordinate system defined by the orthonormal vectors $\hat{\mathbf{x}}$, $\hat{\mathbf{y}}$, and $\hat{\mathbf{z}}$. This coordinate system, of which the origin $\mathbf{r}_0$ is located at the center of the canopy, will be referred to as the reference frame. The radius R and the height H describe the dimensions of V. The canopy volume contains randomly distributed and oriented branches and leaves, the former of which can be classified into N_b different size categories. Their number densities are represented by ρ_b and ρ_l, respectively, where the subscript b is an element of $\{b_1, b_2, \ldots, b_{N_b}\}$ and b_n is used to denote branches of the nth size category.

Incident on the canopy is a vertically polarized wave with wavenumber $k = 2\pi/\lambda$, λ being the wavelength, and direction of propagation $\hat{\mathbf{k}}_i$ relative to the canopy center. The source of this wave is assumed to be located far away from the canopy, so that the incident field amplitude can be approximated as being constant over the canopy volume. The incident wave is scattered in all directions by the scatterers in the canopy volume and the scattered field is observed at a point that is also located far away from the canopy, in the direction $\hat{\mathbf{k}}_s$ relative to the canopy center. The unit vectors $\hat{\mathbf{k}}_i$ and $\hat{\mathbf{k}}_s$ are perpendicular to $\hat{\mathbf{z}}$ and φ_s denotes the azimuthal scattering direction. Without loss of generality, it is assumed that $\hat{\mathbf{k}}_i = \hat{\mathbf{x}}$.

The problem dealt with in Section III is to compute the variance of the (vertical component of the) scattered field due to all branches and leaves. A review of theory concerning the scattering from arbitrarily oriented branches and leaves is provided in Sections II-B and II-C, but the interested reader is referred to [9]–[11] for mathematical details.

B. Scattering From Branches and Leaves

Tree branches are composed of several concentric tissue layers (wood, bark, etc.), each of which is made up of many cells that are much smaller than the wavelengths normally used for mobile communications. It has been shown that the effective dielectric properties of the branch material can be different from one tissue layer to the other, and even anisotropic [12]. However, for simplicity, branches are modeled here as homogeneous dielectrics with effective complex permittivity ϵ_b. Consider a finite-length lossy dielectric cylinder in the

rectangular coordinate system defined by the orthonormal vectors $\hat{\mathbf{x}}'$, $\hat{\mathbf{y}}'$, and $\hat{\mathbf{z}}'$, which will be referred to as the local frame of the cylinder. The cylinder has length h_b and radius r_b and is oriented parallel to $\hat{\mathbf{z}}'$. The scattering of an arbitrarily polarized wave incident on the cylinder can be described in terms of a scattering amplitude tensor, whose elements relate the vertical and horizontal components of the scattered and incident waves, relative to the local frame. If the field inside the cylinder is estimated as the field inside a similar, but infinite cylinder, these tensor elements can be written as in [9, eq. (27)] and [10, eq. (42)].

Leaf material is typically formed by a number of tissue layers, each consisting of many cells of complex composition. However, as the cell dimensions and layer thicknesses are typically much smaller than the wavelength, the interaction of radiowaves with leaves can be well modeled by treating each leaf as a homogeneous dielectric with effective complex permittivity ϵ_l. For a thin circular disk with radius r_l and thickness h_l (h_l small enough that $kh_l[\sqrt{\epsilon_l} - 1] \ll 1$) and with its axis of symmetry aligned with the z'-axis of the local frame, the scattering amplitude tensor elements can be estimated as in [9, eq. (14)] and [11, eq. (47)].

C. Equivalent Scattering Amplitude and Cross Section

The scattering amplitude tensor for a scatterer with an arbitrary, but fixed, orientation with respect to the reference frame, described by the 2-D variable $\Omega = (\alpha, \beta)$, $0 \leq \alpha < 2\pi$, $0 \leq \beta \leq \pi/2$, can be obtained from the corresponding local-frame scattering amplitude tensor by means of a transformation of coordinates. Here, α and β are the azimuthal and elevational rotation angles, respectively, of the local frame relative to the reference frame [10], [11]. In view of the application considered in this paper, we are only interested in the vertical components of the fields incident on and scattered by branches and leaves. The reference-frame scattering amplitude tensor element, which relates these fields, is denoted herein by $F^{b,l}(\hat{\mathbf{k}}_s, \hat{\mathbf{k}}_i)$ and can be computed following [11, eq. (18)]. As previously, the superscripts b and l refer to branches and leaves, respectively.

The probability density functions of the orientations of branches and leaves, relative to the reference frame, are denoted by $f_\Omega^b(\alpha, \beta)$ and $f_\Omega^l(\alpha, \beta)$, respectively. The statistics of α are assumed to be independent of those of β, so that $f_\Omega^{b,l}(\alpha, \beta) = f_\alpha^{b,l}(\alpha) f_\beta^{b,l}(\beta)$. Also, the spatial probability distribution of the scatterers is assumed to be uniform over the canopy volume. The mean scattering amplitude of a single branch or leaf can then be written as

$$\mathrm{E}\left\{F^{b,l}(\hat{\mathbf{k}}_s, \hat{\mathbf{k}}_i)\right\} = \int_0^{2\pi} \int_0^{\frac{\pi}{2}} F^{b,l}(\hat{\mathbf{k}}_s, \hat{\mathbf{k}}_i) f_\Omega^{b,l}(\alpha, \beta) d\beta d\alpha. \quad (1)$$

The equivalent scattering amplitude per unit volume of the canopy is defined as

$$F^{\mathrm{eq}}(\hat{\mathbf{k}}_s, \hat{\mathbf{k}}_i) = \rho_l \mathrm{E}\left\{F^l(\hat{\mathbf{k}}_s, \hat{\mathbf{k}}_i)\right\}$$
$$+ \sum_{b=b_1, b_2, \ldots, b_{N_b}} \rho_b \mathrm{E}\left\{F^b(\hat{\mathbf{k}}_s, \hat{\mathbf{k}}_i)\right\}. \quad (2)$$

In a similar way, the mean scattering cross section of a single branch or leaf is found as

$$4\pi \mathrm{E}\left\{\left|F^{b,l}(\hat{\mathbf{k}}_s, \hat{\mathbf{k}}_i)\right|^2\right\} = 4\pi \int_0^{2\pi} \int_0^{\frac{\pi}{2}} \left|F^{b,l}(\hat{\mathbf{k}}_s, \hat{\mathbf{k}}_i)\right|^2$$
$$\times f_\Omega^{b,l}(\alpha, \beta) d\beta d\alpha \quad (3)$$

and the equivalent scattering cross section per unit volume of the canopy is

$$\sigma^{\mathrm{eq}}(\hat{\mathbf{k}}_s, \hat{\mathbf{k}}_i) = 4\pi \rho_l \mathrm{E}\left\{\left|F^l(\hat{\mathbf{k}}_s, \hat{\mathbf{k}}_i)\right|^2\right\}$$
$$+ 4\pi \sum_{b=b_1, b_2, \ldots, b_{N_b}} \rho_b \mathrm{E}\left\{\left|F^b(\hat{\mathbf{k}}_s, \hat{\mathbf{k}}_i)\right|^2\right\}. \quad (4)$$

Practical values of the number densities and the size, orientation, and dielectric parameters of branches and leaves will be discussed in Section IV-A.

III. SCATTERED FIELD

In general, the fields inside and scattered by a random medium are random functions of position and can be divided into a mean, or coherent, component and a fluctuating component, which is called the incoherent field. As will be shown in Section III-B, under certain reasonable assumptions, the mean intensity of the incoherent tree-scattered field $E_s^{\mathrm{inc}}(\mathbf{r})$ can be expressed in terms of the coherent field intensity inside the canopy. Note that an $e^{j\omega t}$ harmonic time dependence is assumed and suppressed in this section.

A. Coherent Field Intensity Inside the Canopy

The field incident on the canopy can be written as

$$E_i(\mathbf{r}) = A_i(\mathbf{r}) \exp\left\{-j\phi_i(\mathbf{r})\right\} \quad (5)$$

where $A_i(\mathbf{r})$ is the amplitude and $\phi_i(\mathbf{r})$ is the phase. As the source of the incident field is located far away, $A_i(\mathbf{r})$ is considered constant over the canopy volume, i.e., $|E_i(\mathbf{r})| = |E_i(\mathbf{r}_0)|$. It can be shown [13] that the coherent field inside the canopy $\mathrm{E}\{E^{\mathrm{in}}(\mathbf{r})\}$ is governed by an effective propagation constant, given by

$$K = k + \frac{2\pi}{k} F^{\mathrm{eq}}(\hat{\mathbf{k}}_i, \hat{\mathbf{k}}_i) = K' - jK''. \quad (6)$$

Neglecting the reflection and refraction effects at the boundary of the canopy volume, the coherent field intensity inside the canopy is therefore given by

$$\left|\mathrm{E}\left\{E^{\mathrm{in}}(\mathbf{r})\right\}\right|^2 = |E_i(\mathbf{r})|^2 \exp\left\{-2K'' s_1(\mathbf{r})\right\}, \quad \mathbf{r} \in V \quad (7)$$

where

$$s_1(\mathbf{r}) = x + \sqrt{R^2 - y^2}, \quad \mathbf{r} \in V \quad (8)$$

is the length of the path along the incidence direction $\hat{\mathbf{k}}_i$ to $\mathbf{r}$ inside the canopy volume V, as illustrated in Fig. 2.
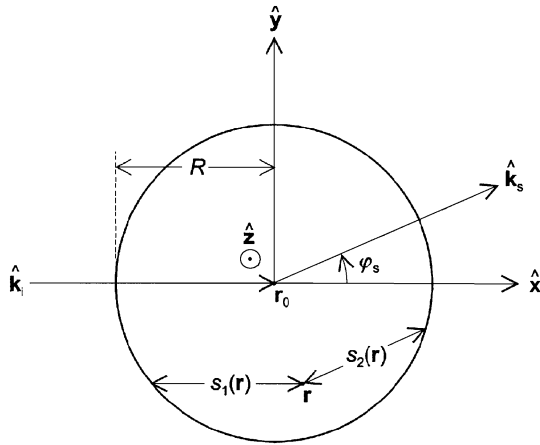
Fig. 2.   Top view of the cylindrical canopy volume V.

As $F^{\mathrm{eq}}(\hat{\mathbf{k}}_i, \hat{\mathbf{k}}_i)$ is in general a complex number, the attenuation constant K'' is nonzero and the coherent field attenuates as it propagates through the canopy. The specific attenuation in decibels per meter (dB/m) is given by

$$\alpha_c = 20 K'' \log_{10} e = 8.686\, K''. \tag{9}$$

B. Incoherent Scattered Field

The incoherent scattered field due to the tree canopy can be obtained from Foldy–Twersky's integral equations in Twersky's multiple scattering theory [13]. This theory takes into account all multiple scattering involving chains of successive scattering going through different scatterers, but neglects the scattering paths that go through a scatterer more than once. According to Twersky's theory, for a uniform density of scatterers, the incoherent scattered field intensity is given by

$$\mathrm{E}\left\{\left|E_s^{\mathrm{inc}}(\mathbf{r})\right|^2\right\} = \int \int \int_V |V(\mathbf{r}, \mathbf{r}')|^2\, \mathrm{E}\left\{\left|E^{\mathrm{in}}(\mathbf{r}')\right|^2\right\} dV'$$
$$\tag{10}$$

in which $V(\mathbf{r}, \mathbf{r}')$ represents the total radiation at $\mathbf{r}$ due to a unit scattering volume at $\mathbf{r}'$, illuminated by a unit-amplitude incident field, through multiple scattering. If the observation point $\mathbf{r}$ is in the far zone of the canopy, $V(\mathbf{r}, \mathbf{r}')$ is well approximated by

$$V(\mathbf{r}, \mathbf{r}') = F^{\mathrm{eq}}(\hat{\mathbf{k}}_s, \hat{\mathbf{k}}_i) \exp\left\{-j(K-k)s_2(\mathbf{r}')\right\} \cdot \frac{e^{-jk|\mathbf{r}-\mathbf{r}'|}}{s}$$
$$\tag{11}$$

where s is the distance from the canopy center to $\mathbf{r}$ and

$$s_2(\mathbf{r}) = -x\cos\varphi_s - y\sin\varphi_s$$
$$+ \sqrt{R^2 - (x\sin\varphi_s - y\cos\varphi_s)^2}, \quad \mathbf{r} \in V \tag{12}$$

is the length of the path from $\mathbf{r}$ along the scattering direction $\hat{\mathbf{k}}_s$, inside V, as illustrated in Fig. 2.

In general, under the assumption that the scatterers in a random medium have a small scattering albedo, the total field intensity $\mathrm{E}\{|E^{\mathrm{in}}(\mathbf{r})|^2\}$ in the medium can be approximated by the coherent intensity $|\mathrm{E}\{E^{\mathrm{in}}(\mathbf{r})\}|^2$. This approximation, and

the substitution of (7) and (11) into (10), lead to the following expression for the incoherent scattered field intensity:

$$\mathrm{E}\left\{\left|E_s^{\mathrm{inc}}(\mathbf{r})\right|^2\right\} = \frac{|E_i(\mathbf{r}_0)|^2}{4\pi s^2}\sigma^{\mathrm{eq}}(\hat{\mathbf{k}}_s, \hat{\mathbf{k}}_i)I(\varphi_s) \tag{13}$$

where

$$I(\varphi_s) = \int \int \int_V \exp\left\{-2K''\left[s_1(\mathbf{r}') + s_2(\mathbf{r}')\right]\right\} dV'. \tag{14}$$

As noted previously, the quasi-two-dimensional model (13) is meaningful only if $s \gg H$. The bistatic scattering cross section of the entire canopy is given by

$$\sigma(\hat{\mathbf{k}}_s, \hat{\mathbf{k}}_i) = \sigma^{\mathrm{eq}}(\hat{\mathbf{k}}_s, \hat{\mathbf{k}}_i)I(\varphi_s). \tag{15}$$

The integral $I(\varphi_s)$ describes to what degree each elemental canopy volume dV' contributes to the total incoherent scattered field and is closely related to the illumination integral in [14]. This integral cannot be evaluated in closed form, but it has been observed empirically that, for small enough K'', a good approximation of $I(\varphi_s)$ is given by

$$I(\varphi_s) = \pi H R^2 \left\{1 + [K''R]^2(1 - \cos\varphi_s)\right\}$$
$$\times \exp\left\{-3.62 K''R + 0.58[K''R]^2\right\}. \tag{16}$$

For $K''R < 1$, this approximation is accurate to within 0.4 dB for all φ_s.

IV. NUMERICAL RESULTS

This section presents numerical results generated using the expressions of the previous section. It also assesses the loss in accuracy caused by the approximation (16). The frequency considered in the computations is 1.9 GHz. Branch and leaf parameters such as size and orientation statistics and dielectric properties are important inputs to the model and will be discussed in Section IV-A.

A. Branch and Leaf Parameters

Number densities, size, and orientation statistics of branches and leaves were analyzed for the oak tree shown in Fig. 3, which is considered to be a typical example of the trees commonly found in urban environments. Branches were categorized into $N_b = 5$ groups according to their radii and for each group the average radius, length, and number density were computed. To this end, the thicker branches (categories 1, 2, and 3) were all counted and measured individually. Radii, lengths, and number densities of the thinner branches (categories 4 and 5), as well as the leaf number density, were determined for a representative section of the canopy. Leaf thickness and radius were measured for a single representative oak leaf. The size parameter values that were thus obtained are listed in Table I. Most of these are larger than the values found by McDonald *et al.* [15] and Karam *et al.* [16] for a walnut orchard. However, the trees examined by these authors were only six years old and, therefore, probably were less mature than the tree analyzed herein and than most urban trees and the tree analyzed in the present study.

Neither branches nor leaves were found to exhibit a preferred azimuthal orientation and the distribution of α is therefore

Fig. 3. Photographs of the oak tree (a) in full leaf (summer) and (b) defoliated (winter).

TABLE I
SIZE AND DIELECTRIC PARAMETERS OF BRANCHES AND LEAVES

Scatterer type	Radius (cm)	Length/thickness (cm)	Relative permittivity	Number density (m^{-3})
Branch (1)	11.4	131	$28 - j7$	0.013
Branch (2)	6.0	99	$28 - j7$	0.073
Branch (3)	2.8	82	$28 - j7$	0.41
Branch (4)	0.7	54	$28 - j7$	5.1
Branch (5)	0.2	12	$28 - j7$	56
Leaf	3.7	0.02	$31 - j8$	420

chosen to be uniform on $(0, 2\pi)$. The statistics of the elevational orientation β of branches and leaves are assumed to be described by the distribution

$$f_\beta^{b,l}(\beta) = \begin{cases} \sin\beta/(\cos\beta_1 - \cos\beta_2), & \text{if } \beta_1 < \beta < \beta_2 \\ 0, & \text{otherwise.} \end{cases} \quad (17)$$

The orientation of the larger branches (categories 1 and 2) was observed to be predominantly vertical and, therefore, these branches are assigned the values $\beta_1 = 0$ and $\beta_2 = \pi/4$. The smaller branches (categories 3, 4, and 5) and the leaves are characterized by $\beta_1 = 0$ and $\beta_2 = \pi/2$, which implies that they have no preferred orientation at all (spherical distribution).

As time did not permit measurements of the effective permittivity of branches and leaves, suitable values were obtained from the literature, as described below. The dielectric properties of branch and leaf material are well known to be strongly influenced by the gravimetric moisture content M_g, defined as the ratio between the mass of the moisture contained in the material and the total mass of the moist material [12]. As the moisture content of branches shows significant diurnal and seasonal variations, their dielectric properties are also strongly time dependent. From the results presented in [15], the average daytime permittivity of branches at 1.2 GHz is found to be $\epsilon_b = 28 - j7$. From a comparison with the dielectric properties of wood, tabulated in [12] as a function of various parameters, it is concluded that ϵ_b remains approximately constant over the range of frequencies used for terrestrial mobile communications and is hardly dependent on temperature above the freezing point.

A semi-empirical formula for the complex permittivity of leaves in terms of M_g and the complex permittivity ϵ_{sw} of saline water, valid in the frequency range from 1 to 100 GHz and for a salinity of about 1%, was proposed in [17] and is written as

$$\epsilon_l = 0.689(M_g - 0.24)\epsilon_{sw} + 4.35 - 3.84 M_g. \quad (18)$$

TABLE II
ATTENUATION COEFFICIENTS ASSOCIATED WITH
BRANCHES AND LEAVES AT 1.9 GHz

Scatterer type	Specific attenuation coefficient (dB/m)
Branch (1)	0.04
Branch (2)	0.08
Branch (3)	0.17
Branch (4)	0.44
Branch (5)	0.07
Leaf	0.30
Total	1.10

For a walnut tree, the moisture content M_g of the leaves was shown in [15] to be time invariant and to have a value of approximately 0.8. The dielectric properties of saline water are strongly dependent on frequency and can be evaluated using [18]. For a frequency of 2 GHz and a salinity of 1%, ϵ_{sw} has a value of $77 - j22$ and the leaf permittivity is $\epsilon_l = 31 - j8$. Similarly to branches, above the freezing point the temperature dependence of ϵ_l is negligible. The dielectric parameter values discussed above are also listed in Table I.

B. Attenuation Coefficients

Theoretical values of the attenuation coefficient α_c, due to the different canopy constituents, computed with the aid of (2), (6), and (9), are shown in Table II. Examination of this table shows that most of the attenuation is due to the smaller branches (size category 4) and the leaves. The total attenuation coefficient for the tree in leaf is 1.10 dB/m; for the defoliated tree, this value is 0.80 dB/m. These values are comparable to, although somewhat lower than, the experimental values published in [7] (1.3 and 1.1 dB/m, respectively), which were obtained in the shadow zone of a single pecan tree at 1.6 GHz. The difference
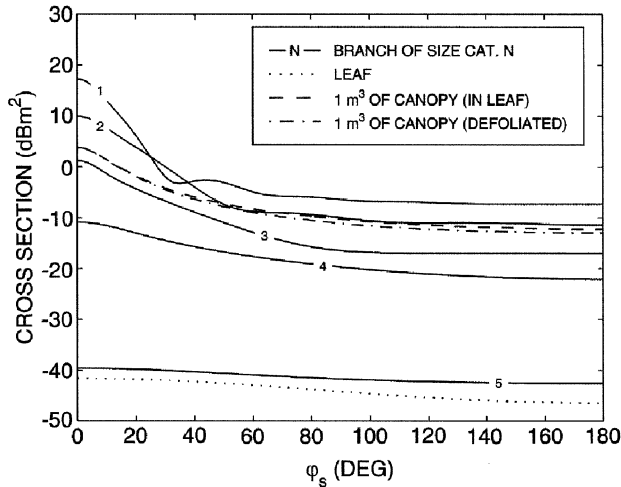
Fig. 4. Mean scattering cross sections of branches and leaves at 1.9 GHz.
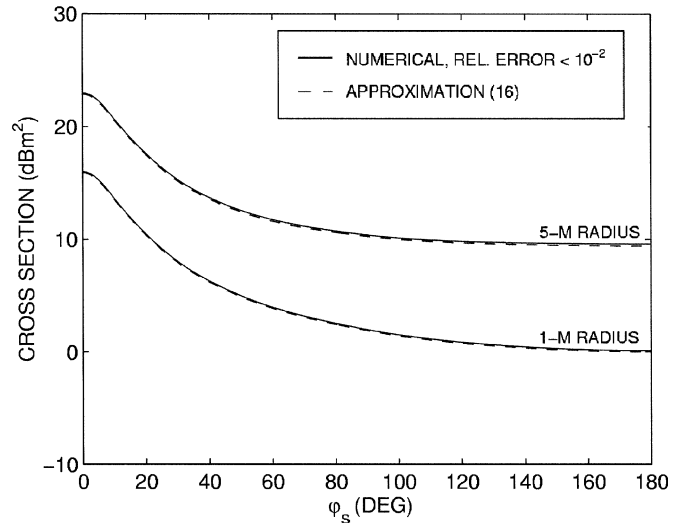

Fig. 5. Theoretical scattering cross sections of a tree (in leaf) at 1.9 GHz, for $R = 1$ m and $R = 5$ m. $H = 8$ m.
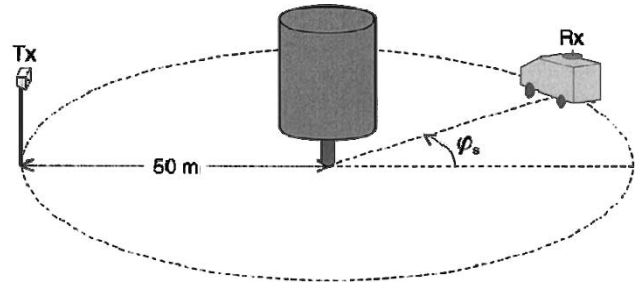

Fig. 6. Illustration of the measurement configuration.

between these values may be related to differences in branch and leaf parameters.

C. Scattering Cross Sections of Branches and Leaves

Fig. 4 shows the mean scattering cross sections for single branches and leaves, computed using (3) with size, orientation, and dielectric parameters taken from Table I. It can be seen that the scattering from the larger branches is concentrated in the forward direction, whereas the scattering from the smallest branches (size category 5) and the leaves is almost isotropic. Fig. 4 also shows the equivalent scattering cross sections per unit volume of canopy $\sigma^{\mathrm{eq}}(\hat{\mathbf{k}}_s, \hat{\mathbf{k}}_i)$ for the tree in full leaf, computed using (4) and the number densities of Table I, and for the defoliated tree, computed by setting $\rho_l = 0$. As can be observed in Fig. 4, $\sigma^{\mathrm{eq}}(\hat{\mathbf{k}}_s, \hat{\mathbf{k}}_i)$ is almost identical for these two cases.

D. Incoherent Scattered Field

To provide insight into the accuracy of the empirical formula (16), the integral $I(\varphi_s)$ in (14) was evaluated numerically with an estimated relative accuracy of 1%, for $R = 1$ and 5 m and $H = 8$ m. Fig. 5 compares the values of $\sigma(\hat{\mathbf{k}}_s, \hat{\mathbf{k}}_i)$ obtained in this way with values generated using (16). The equivalent scattering cross section per unit volume of the canopy $\sigma^{\mathrm{eq}}(\hat{\mathbf{k}}_s, \hat{\mathbf{k}}_i)$ was computed once and then stored for use in the computation of $\sigma(\hat{\mathbf{k}}_s, \hat{\mathbf{k}}_i)$. From Fig. 5, it is seen that the approximation (16) results in a maximum error of approximately 0.2 dB for a canopy radius of 5 m. For a radius of 1 m, the maximum error is approximately 0.1 dB.

V. EXPERIMENTAL RESULTS

This section describes the results of measurements of the field scattered by a single deciduous tree at 1.9 GHz. Where possible, a comparison is made with theoretical results. One of the major concerns with this kind of measurement is the disturbing effects of other multipath contributions entering the receive antenna, of which the direct wave is the most important in the present case. To reduce the effects of scattering from other objects, a tree in the middle of a large, otherwise empty, farmer's field was selected. This tree was described in detail in Section IV-A and is

shown in Fig. 3. To distinguish the scattered field contribution from the direct wave, a wideband channel sounding system, previously described in [19], was employed. With this equipment, multipath waves can be separated on the basis of their propagation delay times.

The measurements were conducted during two periods in different seasons: the first in August and September, 1999, when the tree was in full leaf, and the second in January 2000, when the tree was bare. On all measurement days there was no rain and only a light wind, i.e., leaves were slightly moving, but the branches were still.

A. Measurement Equipment and Procedure

During the experiment, the tree was uniformly illuminated using a 7.1-dBi vertically polarized double-ridged pyramidal horn with an azimuthal 3-dB beamwidth of $53°$. The antenna was located at 7 m above ground level, 50 m away from the center of the canopy, as illustrated in Fig. 6. A rotatable 2-dBi sleeve monopole antenna over a circular ground plane, located on the roof of a measurement vehicle (2.4 m above ground level), was used for reception.

Two types of measurements were conducted, as follows:

1) at a fixed vehicle location, with the antenna moving along a horizontal circle with a radius of 30 cm, which took 16 s to complete one revolution;
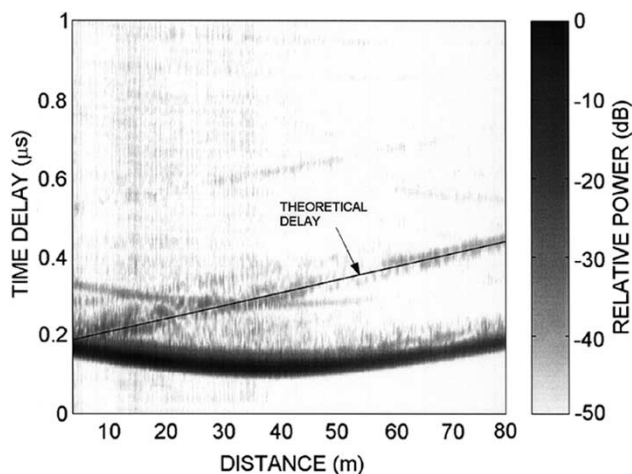2) along a straight trajectory with the receive antenna in a fixed position with respect to the vehicle.

Fig. 7.   Measured power delay profiles along the trajectory $\varphi_s = 135°$.
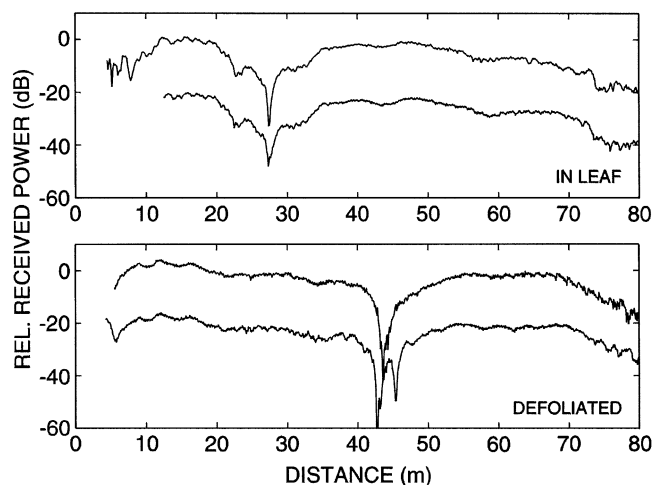

Fig. 8.   Measured field strength, relative to the free-space level, behind the tree in leaf (top) and the defoliated tree (bottom), versus distance from the center of the tree ($\varphi_s = 0°$). Lower curves have an offset of -20 dB for clarity.

While the first type of measurement was used to determine the local average of the scattered power at a number of specific locations, the second was useful to obtain information about the global behavior of the scattered field.

In the experiments of the second type, impulse response data were recorded every 0.1 s while the vehicle was moving at constant speed along a trajectory running radially outward from the center of the tree. As an example, Fig. 7 shows a measured set of power delay profiles for the trajectory corresponding to $\varphi_s = 135°$. In this figure, the direct wave can easily be identified by its hyperbolic shape and because it has minimum delay along the entire trajectory. The solid line represents the theoretical delay associated with the tree-scattered field, which was calculated based on the horizontal path length from the transmitter to the receiver via the center of the tree. This theoretical delay is seen to be in very good agreement with the measured delay of the scattered contribution. The absolute scattered field strength, required to determine the tree's scattering cross section $\sigma(\hat{\mathbf{k}}_s, \hat{\mathbf{k}}_i)$, can be obtained in a way similar to that described in [4]. The weak contribution arriving 0.16 μs after the direct wave for all receiver positions is the result of reflections at the ends of the cable connecting the transmitter unit with the antenna.

In some parts of the area, especially near and behind the tree, the delay difference between the direct and scattered field contributions becomes smaller than the resolution of the channel sounder (20 ns) and the scattered field can no longer be distinguished from the direct field.

B. Attenuation

Fig. 8 shows the received field strength, relative to the free-space level, along a straight trajectory in the shadow area behind the tree ($\varphi_s = 0°$). The results of repeated measurements along the same trajectory are also shown. The field strength is seen to show strong large-scale spatial variations, which are quite different for the in-leaf and the defoliated case, but roughly time invariant between successive measurements. The absence of large small-scale spatial fluctuations indicates that the field behind the tree is predominantly coherent. A possible explanation for the irregular large-scale fading patterns in Fig. 8 is the interference of the wave propagating through the canopy with a ground-reflected wave. For receiver locations close to the tree, the ground-reflected wave propagates *under* the canopy, while at larger distances it is attenuated and phase-shifted by the canopy in the same way as the "direct" wave. The disturbing effect of the ground reflection makes it impossible to verify the theoretical values of the attenuation coefficient α_c, which were found in Section IV-B.

C. Scattering Cross Section

The method described in Section V-A was used to measure the scattered field along a trajectory corresponding to $\varphi_s = 135°$. The reproducibility of the resulting data was verified by repeating the measurement immediately afterward. Fig. 9 shows the scattering cross section $\sigma(\hat{\mathbf{k}}_s, \hat{\mathbf{k}}_i)$, computed from the measured scattered field for every receiver position, versus the distance from the center of the tree. The theoretical value of $\sigma(\hat{\mathbf{k}}_s, \hat{\mathbf{k}}_i)$ for $\varphi_s = 135°$, computed with the aid of (16), is shown for comparison. For this computation, the radius and height of the canopy were chosen equal to 5 and 8 m, respectively.

Although the measured scattering cross section in Fig. 9 does show some large-scale spatial fluctuations, indicating disturbance caused by a ground-reflected wave, its local average value remains approximately constant along the entire trajectory and is very well predicted by the theory. Furthermore, it can be seen that the measurement results for the defoliated case were well reproducible, whereas they appear to have a random time-varying nature for the tree in full leaf. This shows that small movements of leaves can have a significant influence on the instantaneous tree-scattered field.

For the accurate measurement of the scattering cross section as a function of the scattering angle, the mobile receiver was moved to several locations, 10° apart, on the perimeter of a 50-m-radius circle around the canopy center (see Fig. 6). At each location, the receive antenna was rotated along a 30-cm-radius horizontal circle in order to record the local variations of the scattered field. Results of these measurements are given in Fig. 10, which shows the average measured scattering cross section, and the upper and lower 90% percentiles, versus
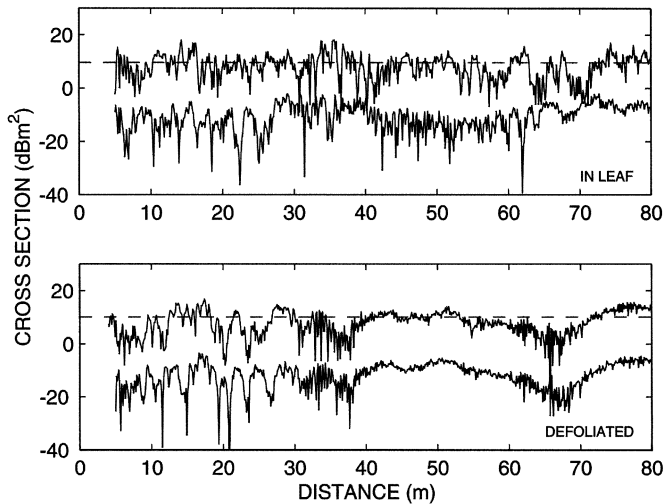
Fig. 9. Measured scattering cross section of the tree in leaf (top) and the defoliated tree (bottom) versus distance from the center of the tree ($\varphi_s = 135°$). Dashed lines represent theoretical values and lower curves have an offset of -20 dB for clarity.
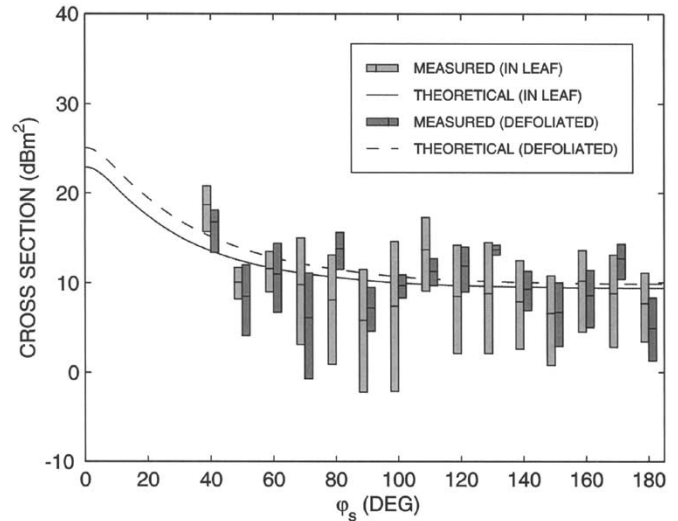

Fig. 10. Measured and theoretical scattering cross section versus the scattering angle. Vertical bars denote average scattered power and upper and lower 90% percentiles.

the scattering angle φ_s. For $\varphi_s < 40°$, the scattered field contribution could no longer be separated from the direct field. Large spreads in the measured cross section are observed over the entire range of φ_s, especially for the tree in leaf. Fig. 10 also shows the theoretical dependence of $\sigma(\hat{\mathbf{k}}_s, \hat{\mathbf{k}}_i)$ on φ_s. Theoretical and average measured values show a good agreement. Discrepancies between the theoretical and measured results can possibly be explained by deviations from the assumed orientation statistics of branches and leaves, particularly the nonuniform orientation distribution of the larger branches over the canopy volume.

Contrary to what might be expected, the theory predicts a larger scattering cross section for the bare tree. Physically, this is because $\sigma^{\text{eq}}(\hat{\mathbf{k}}_s, \hat{\mathbf{k}}_i)$, the equivalent scattering cross section per unit volume of the canopy, is strongly dominated by the branches. Due to the absence of leaves, the incident wave penetrates deeper into the canopy, so that more branches can contribute to the scattered field. The resulting difference in the cross section is small, however, and cannot be confirmed by the experimental results presented in this section.

VI. PROPAGATION PREDICTION RESULTS

The objective of this section is to illustrate how the prediction accuracy of ray-based propagation models can be improved by incorporating the new tree-scattering model. A comparison is made with measured data.

The predictions in this section were generated for an urban environment in Fribourg, Switzerland, at 1.89 GHz. In the past, extensive microcellular-type measurements were conducted in this area and at this frequency [2], [20], [21]. One of the conclusions from these measurements was that the received field strength could not be predicted satisfactorily using a model based only on reflection and diffraction. This was conjectured to be a result of inadequate modeling of the mechanisms responsible for propagation around the street corners, particularly the neglect of tree-scattering effects. The results of this section have served to verify this hypothesis.

The propagation model that produced the predictions is a 2-D ray-tracing model with the following characteristics. Reflected and diffracted fields are computed using the reflection coefficient for impedance boundaries and the diffraction coefficient of Tiberio–Maliuzhinets [22], respectively. In addition, the model considers the incoherent scattering from trees by introducing tree-scattered rays, which interact with the trees at their centers. The field intensities of the scattered ray contributions are computed with the aid of the tree-scattering model proposed in this paper, using (16). Each ray can undergo any possible combination of reflection, diffraction, and scattering, up to a predetermined order. The attenuation of rays passing through tree canopies is also taken into account and is computed as the product of the total path length inside the canopies and the specific attenuation coefficient α_c. The ray-tracing engine makes use of the concept of virtual sources [2] that, together with the real source (the base station antenna), completely describe the field distribution due to the interaction with the environment. The prediction area is divided into square pixels. For each pixel, the local mean power, required to compute the local mean path loss, is obtained using the spatial averaging (SA) method proposed in [23]. The signal contributions due to tree-scattered rays are added noncoherently (in power), however, because their phases are undefined.

The inputs to the model include databases specifying the 2-D coordinates of each building and the locations, radii, and heights of the trees and a table containing the equivalent scattering cross section $\sigma_{\text{eq}}(\hat{\mathbf{k}}_s, \hat{\mathbf{k}}_i)$ per unit canopy volume (cf. Section II-C). The following parameters were used to produce the predictions. The relative permittivity of the buildings ϵ_r was set to 5 and the conductivity was zero. The branch and leaf parameters were taken from Table I. The base station antenna was omnidirectional and the pixel area was $5 \times 5 \text{ m}^2$.

Fig. 11, in which X and Y represent horizontal coordinates, shows area predictions of path loss, with and without considering scattering from trees. The trees, represented by hatched circles, have a radius of 3 m and a height of 8 m. The tree
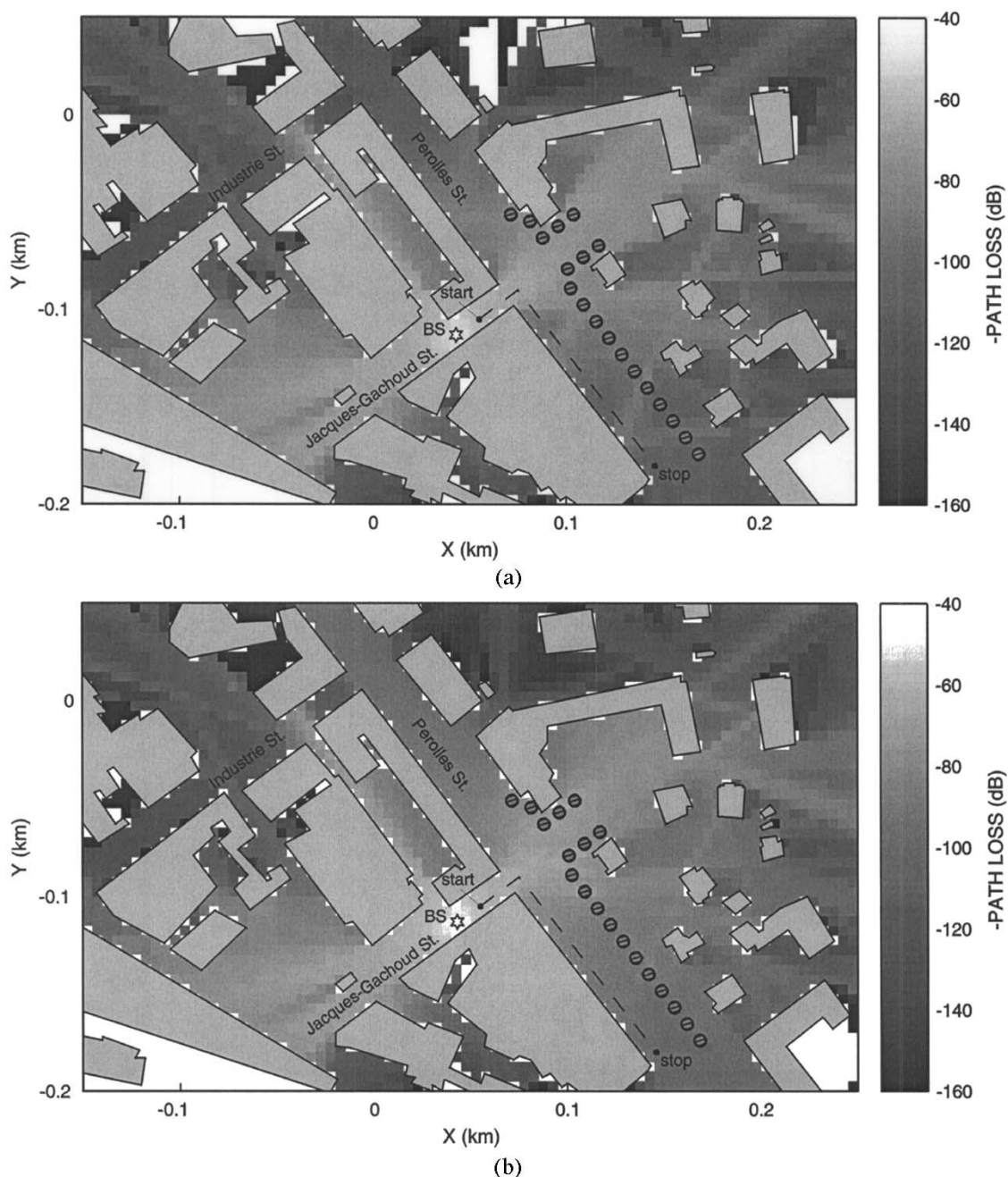
Fig. 11. Area predictions of local mean power for the urban microcell configuration in Fribourg, (a) without and (b) with considering scattering from trees. Predictions were generated considering three reflections and one diffraction. Hatched circles represent trees, and "BS" denotes the base station location.

locations that are indicated in Fig. 11 and are used in generating the predictions are not claimed to be exact, but do represent an adequate picture of the actual situation. The prediction result of Fig. 11(a) was obtained by setting the scattering order to zero, while the result of Fig. 11(b) was generated for scattering order one, allowing maximally one scattering per ray. The reflection order was set to three and the diffraction order was one. The white observation areas (pixels) that can be seen in both subfigures correspond with areas that cannot be "reached" by rays of the order permitted. Distinct differences between the prediction results of Fig. 11(a) and (b) are observed in Perolles Street outside the LoS region. In some parts, these differences amount to over 20 dB. In qualitative terms, the field in Fig. 11(b) appears

to be much more diffused. Propagation around the corners of the intersection is dominated by tree scattering.

A detailed comparison between measured data obtained from [2], [20], and [21][1] and predictions produced with and without taking into account scattering from trees were made for the trajectory indicated in Fig. 11. The number of observation points on this trajectory is 64. Mean and root-mean-square (rms) prediction errors obtained for various ray orders are shown in Table III. This table also shows the number of virtual sources found in the ray-tracing procedure, which gives an indication of the computational complexity. Increasing the

[1] A 10-dB offset must be added to the measured data published in [2] and [20] (cf. [21]).

TABLE III
PREDICTION ERRORS AND NUMBER OF SOURCES FOR URBAN MICROCELL CONFIGURATION IN FRIBOURG, SWITZERLAND, FOR VARIOUS RAY ORDERS

Max. ray order	Number of sources	Mean error (dB)	Rms error (dB)
1 refl., 1 diffr., 0 scatt.	553	-14.9	17.5
2 refl., 1 diffr., 0 scatt.	2,508	-9.9	13.1
3 refl., 1 diffr., 0 scatt.	7,637	-8.6	12.2
4 refl., 1 diffr., 0 scatt.	17,834	-8.4	12.0
5 refl., 1 diffr., 0 scatt.	35,479	-8.3	11.8
6 refl., 1 diffr., 0 scatt.	62,585	-8.3	11.8
7 refl., 1 diffr., 0 scatt.	101,554	-8.3	11.8
1 refl., 1 diffr., 1 scatt.	6,422	-3.9	5.3
2 refl., 1 diffr., 1 scatt.	38,437	-1.9	3.8
3 refl., 1 diffr., 1 scatt.	142,593	-1.5	3.6

reflection order is seen to gradually reduce the prediction error, until convergence is reached at some point. A much larger improvement is achieved, however, by taking into account the effects of tree scattering, which leads to a reduction of the rms prediction error from approximately 12 dB to less than 4 dB, at the cost of an increased computational load. The effects of higher-order tree scattering were not investigated in detail because of the resulting explosive growth in computation time. Fig. 12 shows the measured and predicted path loss along the trajectory, with and without tree scattering. The reflection order is three and the diffraction order is set to one. The improvement due to considering tree scattering is considerable.

VII. CONCLUSION

In this paper, a quasi-two-dimensional model has been presented for the incoherent scattering of radiowaves from a single deciduous tree. This model can be used in conjunction with existing coherent tree-shadowing models that estimate the attenuation associated with propagation through a tree canopy, such as the model in [8]. Incoherent scattering is a mechanism through which a part of the power of an incident field is dispersed in all directions. This can, for example, be an important phenomenon in radio propagation around street corners.

Numerical results from the scattering model were compared with experimental data that were obtained by means of an accurate wideband measurement technique. Measurements of the attenuated field behind the tree were observed to be disturbed by a ground-reflected wave and could not, therefore, be used for a direct verification of the theoretical attenuation due to tree shadowing. Separation of ground-reflected waves from the direct wave is a difficult task for measurement configurations involving low transmit and receive antennas, because they have almost equal propagation delay times and directions of arrival. An alternative method to measure the canopy's specific attenuation, which is complicated but probably more accurate, is to raise one of the antennas to a high level and to use a directive antenna on the other side of the tree to eliminate the ground reflection. Values of α_c that were obtained in this way [7] are in reasonably good agreement with theoretical values found in this paper. Theoretical values of the scattering cross section, which also depend on α_c, were shown to agree well with average measured data.
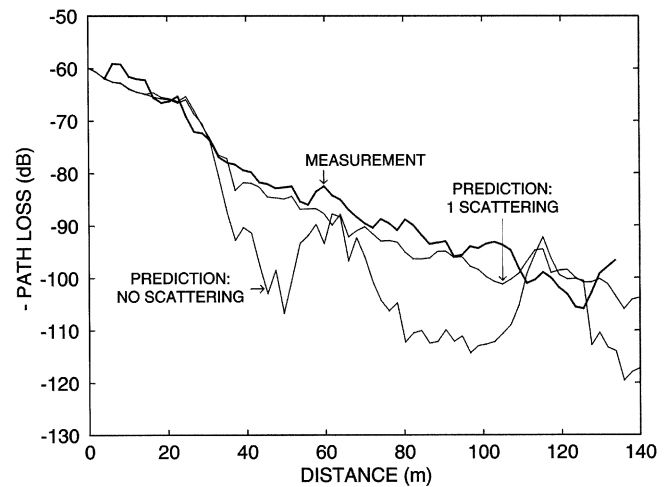

Fig. 12. Measured and predicted path loss along the trajectory. Predictions were generated considering three reflections and one diffraction.

According to the new model, leaves have a considerable influence on the attenuation of radiowaves propagating through the canopy, but hardly make any difference with regard to the tree's scattering cross section. This result, which may at first seem surprising, was in fact verified by the experimental results discussed in Section V-C, which showed little difference between the scattering cross section of a bare tree and the same tree in full leaf. From the viewpoint of radio-network planning, this is a convenient result because it implies that (incoherent) tree scattering models need not be season dependent.

The new scattering model is unable to predict the considerable spatial fluctuations of the scattered field that were observed in the measurements. Indeed, it is likely that the unpredictability of these variations cannot be overcome by any model, however sophisticated. Still, as the present model is capable of providing accurate average values of the scattered field, it can significantly improve the accuracy of propagation prediction for vegetated urban environments.

ACKNOWLEDGMENT

REFERENCES

[1] V. Erceg, A. J. Rustako, and R. S. Roman, "Diffraction around corners and its effects on the microcell coverage area in urban and suburban environments at 900 MHz, 2 GHz, and 6 GHz," *IEEE Trans. Veh. Technol.*, vol. 43, pp. 762–766, Aug. 1994.

[2] K. Rizk, J.-F. Wagen, and F. Gardiol, "Two-dimensional ray tracing modeling for propagation prediction in microcellular environments," *IEEE Trans. Veh. Technol.*, vol. 46, pp. 508–518, May 1997.

[3] Y. L. C. de Jong, M. H. A. J. Herben, J.-F. Wagen, and A. Mawira, "Transmission of UHF radiowaves through buildings in urban microcell environments," *Electron. Lett.*, vol. 35, no. 9, pp. 743–745, 1999.

[4] Y. L. C. de Jong, M. H. J. L. Koelen, and M. H. A. J. Herben, "Measurement of building transmission loss using wideband radio channel sounding," *Electron. Lett.*, vol. 36, no. 12, pp. 1067–1069, 2000.

[5] ——, "A building transmission model for improved propagation prediction in urban microcells," *IEEE Trans. Veh. Technol.*, vol. 53, pp. 490–502, Mar. 2004.

[6] Y. L. C. de Jong, "Measurement and Modeling of Radiowave Propagation in Urban Microcells," Ph.D. dissertation, Eindhoven University of Technology, Eindhoven, The Netherlands, 2001.

[7] W. J. Vogel and J. Goldhirsh, "Earth–satellite tree attenuation at 20 GHz: foliage effects," *Electron. Lett.*, vol. 29, no. 18, pp. 1640–1641, 1993.

[8] S. A. Torrico, H. L. Bertoni, and R. H. Lang, "Modeling tree effects on path loss in a residential environment," *IEEE Trans. Antennas Propagat.*, vol. 46, pp. 872–880, June 1998.

[9] M. A. Karam, A. K. Fung, and Y. M. M. Antar, "Electromagnetic wave scattering from some vegetation samples," *IEEE Trans. Geosci. Remote Sensing*, vol. 26, pp. 799–808, Nov. 1988.

[10] M. A. Karam and A. K. Fung, "Electromagnetic scattering from a layer of finite length, randomly oriented, dielectric, circular cylinders over a rough interface with application to vegetation," *Int. J. Remote Sensing*, vol. 9, no. 6, pp. 1109–1134, 1988.

[11] ——, "Leaf-shape effects in electromagnetic wave scattering from vegetation," *IEEE Trans. Geosci. Remote Sensing*, vol. 27, pp. 687–697, Nov. 1989.

[12] G. I. Torgovnikov, *Dielectric Properties of Wood and Wood-Based Materials*. Berlin, Germany: Springer-Verlag, 1993.

[13] A. Ishimaru, *Wave Propagation and Scattering in Random Media*. New York: Academic Press, 1978.

[14] F. T. Ulaby, T. E. van Deventer, J. R. East, T. F. Haddock, and M. E. Coluzzi, "Millimeter-wave bistatic scattering from ground and vegetation targets," *IEEE Trans. Geosci. Remote Sensing*, vol. 26, pp. 229–243, May 1988.

[15] K. C. McDonald, M. C. Dobson, and F. T. Ulaby, "Using MIMICS to model L-band multiangle and multitemporal backscatter from a walnut orchard," *IEEE Trans. Geosci. Remote Sensing*, vol. 28, pp. 477–491, July 1990.

[16] M. A. Karam, A. K. Fung, R. H. Lang, and N. S. Chauhan, "A microwave scattering model for layered vegetation," *IEEE Trans. Geosci. Remote Sensing*, vol. 30, pp. 767–784, July 1992.

[17] C. Mätzler, "Microwave (1–100 GHz) dielectric model of leaves," *IEEE Trans. Geosci. Remote Sensing*, vol. 32, pp. 947–949, Sept. 1994.

[18] F. T. Ulaby, R. K. Moore, and A. K. Fung, *Microwave Remote Sensing: Active and Passive*. Dedham, MA: Artech House, 1986, vol. 3, Appendix E.

[19] Y. L. C. de Jong and M. H. A. J. Herben, "High-resolution angle-of-arrival measurement of the mobile radio channel," *IEEE Trans. Antennas Propagat.*, vol. 47, pp. 1677–1687, Nov. 1999.

[20] K. Rizk, "Propagation in Microcellular and Small Cell Urban Environment," Ph.D. dissertation, Ecole Polytechnique Fédérale de Lausanne, Lausanne, Switzerland, 1997.

[21] J.-F. Wagen and K. Rizk, "Ray tracing based prediction of impulse responses in urban microcells," in *Proc. IEEE 44th Veh. Technol. Conf. (VTC'94)*, Stockholm, Sweden, 1994, pp. 210–214.

[22] R. Tiberio, G. Pelosi, and G. Manara, "A uniform GTD formulation for the diffraction by a wedge with impedance faces," *IEEE Trans. Antennas Propagat.*, vol. AP-33, pp. 867–873, Aug. 1985.

[23] Y. L. C. de Jong and M. H. A. J. Herben, "Prediction of local mean power using 2-D ray-tracing-based propagation models," *IEEE Trans. Veh. Technol.*, vol. 50, pp. 325–331, Jan. 2001.

Yvo L. C. de Jong (S'96–M'01) received the M.Sc. (*cum laude*) and Ph.D. degrees in electrical engineering from the Eindhoven University of Technology, Eindhoven, The Netherlands, in 1996 and 2001, respectively.

He was with KPN Research (now TNO Telecom), Leidschendam, The Netherlands, from 1997 to 1998, in the framework of his Ph.D. dissertation work on deterministic propagation modeling for mobile communications. He visited Swisscom Corporate Information and Technology, Bern, Switzerland, in 1998. In 2001, he joined the Communications Research Centre Canada (CRC), Ottawa, as a Research Scientist. His current research interest is in the area of multiple-input–multiple-output (MIMO) wireless systems.

Dr. de Jong's Ph.D. dissertation was nominated for the 2002 Telecommunication Award of the Dutch Royal Institute of Engineers (KIvI) and was awarded the second prize.

Matti H. A. J. Herben (S'80–M'83–SM'88) was born in Klundert, The Netherlands, in 1953. He received the M.Sc. degree (*cum laude*) in electrical engineering and the Ph.D. degree in technical sciences from Eindhoven University of Technology (EUT), The Netherlands, in 1978 and 1984, respectively.

Since 1978, he has been with the Radiocommunications Group of EUT, currently as an Associate Professor. His research interests and publications are in the areas of the design and numerical analysis of reflector and lens antenna systems, radio interference reduction, electromagnetic wave propagation on terrestrial and satellite links, remote sensing of the turbulent troposphere, and microwave radiometry.

Dr. Herben is a Member of the Royal Institute of Engineers (KIvI), the Netherlands Electronics and Radio Society (NERG), and the Dutch URSI Committee. He was an Associate Editor of *Radio Science* from 1993 to 1996.